Empirical fragility curves for settlement-affected buildings

Analysis of different intensity parameters for seven hundred masonry buildings in The Netherlands

Peduto, Dario; Korff, Mandy; Nicodemo, Gianfranco; Marchese, Antonio; Ferlisi, Settimio

DOI
10.1016/j.sandf.2018.12.009

Publication date
2019

Document Version
Accepted author manuscript

Published in
Soils and Foundations

Citation (APA)
Peduto, D., Korff, M., Nicodemo, G., Marchese, A., & Ferlisi, S. (2019). Empirical fragility curves for settlement-affected buildings: Analysis of different intensity parameters for seven hundred masonry buildings in The Netherlands. *Soils and Foundations*, *59*(2), 380-397. https://doi.org/10.1016/j.sandf.2018.12.009

PAPER TITLE

Empirical fragility curves for settlement-affected buildings: analysis of different intensity parameters for seven hundred masonry buildings in The Netherlands

Authors: Dario Peduto[a], Mandy Korff[b,c], Gianfranco Nicodemo[a], Antonio Marchese[a], Settimio Ferlisi[a]

[a] Department of Civil Engineering
University of Salerno
via Giovanni Paolo II, 132
84084 - Fisciano (SA), Italy
e-mail: dpeduto@unisa.it; gnicodemo@unisa.it; amarchese@unisa.it; sferlisi@unisa.it

[b] Deltares
P.O BOX, 177
2600 MH Delft, The Netherlands
e-mail: mandy.korff@deltares.nl

[c] Delft University of Technology,
Faculty of Civil Engineering and Geosciences
Building 23, Stevinweg 1 / PO-box 5048
2628 CN Delft / 2600 GA Delft, The Netherlands
e-mail: M.Korff@tudelft.nl

Corresponding author:

*Settimio Ferlisi

Department of Civil Engineering, University of Salerno
via Giovanni Paolo II, 132
84084 - Fisciano (SA), Italy
e-mail: sferlisi@unisa.it
Office: +39 089964317; Mobile: +39 3204226928

Abstract

The analysis and prediction of damage to buildings resting on highly compressible fine-grained "soft soils" containing (organic) clays and peat are key issues to be addressed for a proper management of subsidence-affected urban areas. Among the probabilistic approaches suggested by literature, those oriented to the generation of empirical fragility curves are particularly promising provided that a comprehensive dataset on both subsidence-related intensity (SRI) parameters and corresponding damage severity to buildings is available. Following this line of thought, in this paper a rich sample of more than seven hundred monitored (by remote sensing) and surveyed masonry buildings – mainly resting with their (shallow or piled) foundations on soft soils – is analyzed in four urban areas in The Netherlands. Probabilistic functions in the form of fragility curves for building damage are retrieved for three different SRI parameters (i.e. differential settlement, rotation and deflection ratio) derived from the processing of Synthetic Aperture Radar (SAR) images by way of a differential interferometric (DInSAR) technique in combination with severity levels of damage recorded from visual inspection of over 700 masonry buildings. As a novelty with respect to earlier similar studies, the work points out the methodological steps to be followed in order to identify the most appropriate SRI parameter among the selected ones. Thus, the objective of the paper is to improve the existing geotechnical forecasting tools for subsidence-affected urban areas, in order to target areas that require more detailed investigations/analyses and/or selecting/prioritizing foundation repairing/replacing measures.

Keywords: Soft soils, Settlements, Shallow/piled foundations, Fragility curves, DInSAR

1. INTRODUCTION

Ground settlements related to subsidence phenomena of either natural or anthropogenic origin, or complex combinations of both, yearly cause damage to affected facilities (e.g. buildings) resulting in economic losses of billions of US Dollars per year (Holzer 2009; Bucx et al. 2015). For this reason, scientists, technicians, politicians and civilian communities are interested in studies aimed at analyzing and predicting the consequences to buildings in subsiding areas in order to select the most suitable strategies for land-use planning and urban management purposes. The availability of information on the spatial distribution and severity of damage suffered by buildings, as well as their displacement rates, is crucial in the above studies. In addition to conventional monitoring techniques like topographic leveling, tachymetry, and global navigation satellite systems (GNSS), useful information on displacement rates can derive from processing images acquired by spaceborne Synthetic Aperture Radar (SAR) sensors via advanced differential interferometric techniques (generically called "DInSAR"). DInSAR-derived displacement rates are currently available over a large number of buildings and recent works by the authors (Peduto et al. 2016a, 2017c, 2018b) show that they can be successfully combined with the results of damage surveys to generate empirical fragility curves. These latter, as a rule, provide the conditional probability of reaching or exceeding a certain damage severity level as a function of a subsidence-related intensity (SRI) parameter that affects a generic (i.e. randomly selected) building – belonging to a homogeneous set of surveyed buildings – over a given period of time.

The key idea of the present work is to evaluate the use of different SRI parameters – whereas previous works focused on one parameter only (Peduto et al. 2016a, 2017c) – by carrying out a feasibility test aimed at identifying the SRI parameter (amongst three) that best fits the damage analysis and prediction for large quantities of houses. In particular, the procedure introduced by Peduto et al. (2017c) was improved to derive (from DInSAR data) the investigated SRI parameter – i.e. differential settlement, rotation and deflection ratio (Burland and Wroth 1974) – to be combined with a rich dataset of information gathered from in-situ damage surveys over more than seven

hundred masonry buildings with both shallow and piled foundations in four cities in subsiding areas in The Netherlands.

The selected cities are situated in areas that suffer from widespread ground settlements (Papadaki 2013) mainly associated with the presence of highly compressible fine-grained "soft soils", e.g. clay and peat in the upper strata (Den Haan and Kruse 2006). The subsidence-related problems are often exacerbated by decay processes (due to fungal or bacteria attack) affecting wooden piles (Klaassen and Creemers 2012). Foundations in the study area consist of both shallow and piled systems, whose functionality under live loads can be so seriously compromised that, with the passing of time, costly maintaining/repairing/replacing measures have to be undertaken in order to prevent building serviceability/ultimate limit states.

2. DAMAGE ASSESSMENT AND CLASSIFICATION

Empirical relationships between displacements of foundations and damage induced to superstructures have been developed by several researchers. Early on, Skempton and MacDonald (1956) reported observations of settlements and onsets of cracking to 98 buildings with isolated/continuous footings resting on fine-/coarse-grained soils; while Polshin and Tokar (1957) suggested a damage criterion based on 25 years of Soviet experience. Bjerrum (1963) first retrieved useful relationships between the maximum settlement and the maximum differential settlement, and recommended limiting values of angular distortions for buildings. Grant et al. (1974) enlarged the settlement and damage database (available at that time) with an additional sample of 95 buildings. Burland and Wroth (1974) addressed the conditions leading to settlement-induced damage and, similar to Polshin and Tokar (1957), concluded that visible cracking relates to exceedance of certain values of tensile strains.

Based on the damage criteria mentioned above, limiting values of some SRI parameters (e.g. angular distortion/relative rotation) are currently used in several design codes (AASHTO 1997, CEN 2004).

The state of the art on building damage for masonry buildings is mainly based on the work of Boscardin and Cording (1989) and Burland (1995) and is more commonly known as the Limiting Tensile Strain Method (LTSM). This method is generally adopted in case of tunneling or other ground related works. The LTSM involves classifying the damage severity according to the system proposed by Burland et al. (1977) for brickwork or blockwork and stone masonry, which mainly reflect the attainment of damage affecting the building aesthetics (D0 = negligible, D1= very slight and D2 = slight), causing a loss of functionality (D3 = moderate and D4 = severe) or even compromising the stability (D5 = very severe). According to LTSM, a given damage severity level is attained if the combination of bending, shear and horizontal strain (combined in one tensile strain) reaches a certain limiting value. Factors influencing the limit values of the tensile strain are for example the geometrical and mechanical characteristics of the building (Son and Cording, 2007).

The main question that this paper aims to address is whether these approaches also work for large numbers of buildings for which limited information is available. Considering the inherent uncertainties involved in the problem, an interesting perspective is offered by probabilistic tools relating different (measured) SRI parameter values with (surveyed) damage severity levels in the form of empirical fragility curves. For these latter, following an approach adopted in the earthquake engineering field (Gehl et al. 2015, Shinozuka et al. 2000) a lognormal distribution is usually assumed (Ferlisi et al. 2018; Peduto et al. 2016a,b, 2017a,c; Saeidi et al. 2012):

$$P(Damage \geq Di|SRI) = \Phi\left[\frac{1}{\beta_i} ln\left(\frac{SRI}{\overline{SRI}_i}\right)\right] \quad (1)$$

where $P(\cdot)$ is the probability of reaching/exceeding a certain damage severity level Di for a given value of SRI, $\Phi[\ ]$ is the standard normal cumulative distribution function, $\overline{SRI}_i$ and β_i respectively represent the median and the standard deviation (or fragility parameters according to Shinozuka et al. 2003) of the lognormal distribution for each damage severity level, Di.

3. DInSAR DATA AND ACCURACY TEST

Spaceborne Synthetic Aperture Radar (SAR) images processed via advanced differential Interferometric techniques (DInSAR) are currently widely used to detect and analyze ground displacements associated with either natural or anthropogenic phenomena. Some recent pioneering examples of application in geotechnical modelling have combined subsoil and settlement modelling with the information gathered by DInSAR-derived ground displacements (Castaldo et al., 2015; Modoni et al., 2013; Peduto et al., 2017b). In this work, Persistent Scatterers Interferometry (PSI) (Costantini et al. 2008; Ferretti et al. 2001) techniques are used to identify reliable scatterers (e.g. buildings). In particular, these PSI-retrieved displacements are provided, with reference to a ground point, along the radar line of sight (LOS) with a sub-millimeter precision (Hanssen 2003) or accuracy (Nicodemo et al. 2016; Peduto et al. 2017b, 2018a) on the average velocity and sub-centimeter accuracy on the single displacement measurement (Herrera et al. 2009). For the specific purpose of ground displacement monitoring in built-up urban areas, X-band high-resolution SAR sensor TerraSAR-X (TSX) and COSMO-SkyMed recently proved to be suitable for precise monitoring of single structures/infrastructure (Cascini et al. 2013; Fornaro et al. 2013, 2014; Nicodemo et al. 2016; Peduto et al. 2015, 2017b,c, 2018a; Reale et al. 2011; Zhu and Bamler 2010). In the present study, the availability of a large quantity of both DInSAR and topographic leveling data on the Schiedam-West neighborhood in the city of Schiedam (The Netherlands) allowed carrying out an accuracy test of the used dataset. This latter consists of 285 images (133 on ascending orbit and 162 on descending orbit) acquired via the stripmap mode by the TerraSAR-X constellation of satellites spanning the period 2009-2014 (Peduto et al. 2017c). Moreover, long-term measurements from four hundred leveling benchmarks on building façades are available. These data, covering ten years starting from 2004, are filtered in the same period of DInSAR data (2009-2014) and only levelling time series with a minimum frequency of one measurement per year are considered for the comparison. Then, permanent scatterers (PS) within a 2 m spatial buffer around the single leveling point are selected in order to take into account the localization error of DInSAR

measurements. Adopting these criteria, 83 levelling benchmarks are used in the analysis and their velocity values over the observation period are compared with the average velocity value of all selected PS (on both ascending and descending orbit) falling within the 2 m buffer around the levelling point (Fig. 1a). The accuracy of DInSAR velocity for the test area is computed in terms of the difference between DInSAR and levelling data (ΔV) for each considered benchmark. A histogram of the DInSAR accuracy is shown in Fig. 1b, with an average value equal to 0.85 mm/year and standard deviation of 0.55 mm/year. Accordingly, the 1-sigma accuracy can be set to 1.40 mm/year, thus confirming for the case study at hand the results from other authors (e.g. Herrera et al. 2009; Peduto et al. 2018a).

For the sake of completeness, the relationship between the quality parameter of the PS dataset and ΔV values is also investigated. The PS quality parameter is representative of the conformity (namely coherence) between the measured DInSAR data and the displacement model used in the DInSAR analysis phase. It can range from 0 (points lacking conformity with the model and which are therefore unreliable) to 1 (points with high conformity with the model and which are therefore reliable). A low coherence value does not necessarily indicate a high noise level of the data but can be caused by types of motion that deviate from the linear motion model. As shown by the diagrams in Figure 1c, it is possible to derive which ΔV average value and related standard deviation are expected for a given range of the quality parameter. Indeed, the ΔV value decreases as the quality parameter increases; therefore the higher the quality parameter is the more accurate DInSAR data are. This means that DInSAR data are considered accurate enough to derive the fragility curves for the different building and foundation types.

4. METHODOLOGY

The procedure followed for the analyses consists of three phases preceded by a preliminary data preparation phase (Fig. 2). In particular, the PSI data are separated between PS on top of buildings and PS at ground level and the accuracy test described in section 3 is carried out in order to check if

the limiting value proposed in literature (i.e. 1.5 mm/year) is satisfied. Then, if the PS on top of buildings fall within a 2-meter buffer around the building's perimeter, they are associated with that building (Fig. 3a). In phase I-A, the cumulative settlement pertaining to each PS over the observation period is derived by multiplying the available PS velocity by the monitoring period. In this way, settlements are implicitly assumed as occurring at a constant rate in the study area during the observation period. This assumption is acceptable if we consider that such widespread settlements in the analyzed areas mainly relate to long-term creep processes (Den Haan and Kruse 2006, Peduto et al. 2017c). PS-derived settlement data are interpolated over each building on a 2 m × 2 m grid so that settlement profiles can be retrieved along selected sections, i.e. parallel to the road in the case study at hand as shown in Figure 3a.

Once the settlement profile is derived, different SRI parameters of foundation movement are computed. It is worth stressing that settlements refer to PS located on the building roof but, hereafter in the study, they are considered as occurring at the foundation level, thus neglecting either compressive or tensile strains that may affect the superstructure (Cascini et al. 2007). Accordingly:

- the differential settlement $\delta\rho$ is computed along the profile as the difference between maximum and minimum values of recorded settlements (Fig. 3b);
- the rotation (θ), or slope, is assumed as $\theta = \delta\rho/L_\rho$, where L_ρ indicates the distance at the foundation level between the two points where $\delta\rho$ was computed (Fig. 3b);
- the deflection ratio is obtained as Δ/L according to the definitions provided by Burland and Wroth (1974), where Δ is the displacement of a point relative to the line connecting two reference points and L is the distance between these two points.

For the evaluation of the deflection ratio, the location of the reference points is critical. Since it is not straightforward defining the position of these points from DInSAR data, two different values of the deflection ratio (Δ_1/L_1 and Δ_2/L_2) are defined in the present analysis (Figs. 3c-d) as follows:

1. in the simplified approach the deflection ratio is given by Δ_1/L_1, being Δ_1 the displacement of a point relative to the line connecting two consecutive points of intersection between the line (that joins the two extremities of the building foundation with a distance L) and the settlement profile; whereas L_1 is the distance between two consecutive points of intersection. In particular, as shown in Figure 3c, the value of $(\Delta_{1s}/L_{1s})_{max}$ and of $(\Delta_{1h}/L_{1h})_{max}$, respectively in the sagging and hogging zones, are estimated for every building and the biggest value of these two $[(\Delta_1/L_1)_{max} = \max\{(\Delta_{1s}/L_{1s})_{max}; (\Delta_{1h}/L_{1h})_{max}\}]$ is associated with the corresponding damage severity level of a given building, taking into account that a single damage severity level was identified for a single building.
2. The standard/original approach for the deflection ratio – according to the definition provided by Burland and Wroth (1974) – is obtained as Δ_2/L_2 being Δ_2 the displacement of a point relative to the line connecting two consecutive inflection points; whereas L_2 is the distance between two consecutive points of inflection (see also Burland et al. 2004, Franzius et al. 2004). In Figure 3d, the value of $(\Delta_{2s}/L_{2s})_{max}$ and of $(\Delta_{2h}/L_{2h})_{max}$ – respectively, in the sagging and hogging zones – are estimated for every building and the biggest value of these two $[(\Delta_2/L_2)_{max} = \max\{(\Delta_{2s}/L_{2s})_{max}; (\Delta_{2h}/L_{2h})_{max}\}]$ is associated with the corresponding damage severity level of a given analyzed building.

A further essential step is the use of visually obtained damage surveys (phase I-B). For this purpose, the fact-sheets to be filled-in during the in-situ surveys (Peduto et al. 2017c) allow collecting information about the location of a certain building and its description in terms of structural type, foundation typology (i.e. shallow or piled), number of floors, age of construction and occupancy type, the available datasets on geological features and PSI data, the photos of damage experienced by the building façades (in terms of cracks and/or disjunction in the outer walls and their position, distortions or tilt) and, finally, the damage severity level assigned on the basis of the classification system provided by Burland et al. (1977).

In Phase II, empirical relationships between the magnitude of the selected SRI parameters and the level of damage severity assigned during surveys for all the analyzed (706) masonry buildings with shallow or piled foundations are developed.

In Phase III, using Eq. (1) empirical fragility curves are generated and evaluated for different SRI parameters pertaining to masonry buildings resting on either shallow or piled foundations.

The fragility parameters (i.e. $\overline{SRI}_i$ and β) are computed following the procedure proposed by Shinozuka et al. (2003). In particular, a unique β value is adopted in order to have coherent probabilities for the different damage level (Fotopoulou et al. 2013). The maximum likelihood (ML) method is used to estimate the fragility parameters as those that maximize the likelihood of fitting with "real" data. As β is taken equal for all damage levels, the likelihood function can be expressed as (Mavrouli et al. 2014; Shinozuka et al. 2003):

$$L(\overline{SRI}_i, \beta) = \prod_{j=1}^{N} \prod_{i=0}^{k} P_i\left(SRI_j; D_i\right)^{y_{ji}} \quad (2)$$

where $P_i = P(SRI_j, D_i)$ is the probability that the *j*-th (randomly selected) building from the sample will be in the damage level D_i when subjected to SRI_j parameter value; D_i in turn indicates the considered damage severity level with *i* ranging from 0 to *k* (*k* = 0,1,2,3 for the sample of buildings resting on shallow foundations and *k* = 0,1,2,3,4 for buildings with piled foundations); $y_{ji} = 1$ if the damage level D_i occurs for the *j*-th building subjected to SRI_j intensity value, $y_{ji} = 0$ otherwise.

Finally, the fragility parameters are obtained by solving the following equations to maximize the likelihood function (Shinozuka et al. 2003):

$$\frac{\partial lnL(\overline{SRI}_i,\beta)}{\partial \overline{SRI}_i} = \frac{\partial lnL(\overline{SRI}_i,\beta)}{\partial \beta} = 0 \quad (3)$$

5. CASE STUDY AREAS

The Netherlands, a low-lying river delta close to the North Sea, has a number of distinct geographic regions determined by their dominant soil profile (Hartemink and Sonneveld 2013). About half of

the country's surface is found below the sea level ("Normal Amsterdam Level", N.A.P.). The four main rivers (Rhine, Meuse, Scheldt and IJssel) and the sea have shaped the Dutch Holocene depositionary environment. As a result, the subsoil consists of highly compressible soils in the western and northern regions (Fig. 4); to the east, Pleistocene deposits – mainly made up of sandy soils sloping upwards to the south (van der Meulen et al. 2013) – prevail. In the last decades, the Geological Survey of The Netherlands (GDN) has systematically collected and analyzed hundreds of thousands of borehole data and cone penetration tests (Stafleu et al. 2011) that allowed generating the nationwide 3D geological 'GeoTOP' model (DINOloket 2016). In particular, this model schematizes the Dutch subsoil in millions of voxels (100 × 100 × 0.5 m, height × width × depth) providing information on the litho-stratigraphy (including the probability of occurrence of each lithological class) down to a depth of 50 m below the ground surface.

In the present study, 706 masonry buildings with shallow and (mainly wooden) piled foundations belonging to four municipalities are analyzed (Fig. 4): Zaanstad, Rotterdam, Schiedam, Dordrecht. These municipalities are all located within the areas where large deposits of soft soils are present. The building stock analyzed consists of low-rise masonry buildings (2-3 floors), whose age dates back to the beginning of the 19th century up to about the 1980s, mainly constructed out of brick and lime mortar.

As for DInSAR data used for the analyses, they were provided by SkyGeo Netherlands B.V. that developed a commercial chain 'Antares' – mainly based on the PSI method (Ferretti et al. 2001) – for processing SAR images, in this case acquired by the TerraSAR-X satellite constellation via the stripmap mode. As an input Digital Elevation Model (DEM), the SRTM90 (USGS 2016) was used. Considering the flatness of Dutch topography, the DEM resolution is sufficient for unambiguous height estimation (Bamler and Hartl 1998) and subsequent estimation of atmospheric disturbances (Ferretti et al. 2001). Since subsidence-related displacements are assumed as mainly vertical, the PSI data were projected from the LOS to the vertical direction (Cascini et al. 2007).

5.1 Zaanstad

Zaanstad is a densely urbanized municipality located north of Amsterdam. A generic cross-section along the A-A' profile (Fig. 5a) shows that in Zaanstad area the upper part of the subsoil consists of mainly clay and peat with a cumulative thickness not exceeding 10 m, resting on a sandy deposit that includes some thin lenses of clayey soils or sandy clay (Peduto et al., 2016a). Consequently, in the historic centre of Zaanstad the masonry buildings mainly rest on wooden piles in order to prevent loading the upper highly compressible layers. This town, like most western cities of The Netherlands, suffers from widespread building foundation problems that prompted the municipality to arrange extensive campaigns for foundation inspections aimed at investigating their conservation state. The results of the inspections highlighted that several piled foundations suffered from the effects of wood decay so that restoration works were promoted.

The available SAR image dataset over Zaanstad consists of 162 TSX images acquired via the stripmap mode on the ascending orbit between 05 February 2009 and 14 October 2015.

Figure 5b shows PSI data over the two selected parts of Zaanstad that exhibited the highest settlement rates in the period of observation. In Figure 5c the map of the buildings that were surveyed between February and March 2016 is shown. All eighty-one buildings surveyed rest on piles. Figures 5e and 5f show some photos of the buildings; Figure 5d displays the distribution of damage level. The number of buildings per damage severity level is: D0 = 8; D1 = 31; D2 = 20; D3 = 16; D4 = 6; D5 = 0.

5.2 Rotterdam

The city of Rotterdam is located in the southwestern part of The Netherlands (Fig. 6a), in the area that is part of the Rhine-Meuse delta system. The upper 20 m of subsurface consist of unconsolidated, Holocene sediments, deposited in fluvial and coastal environments. As shown in Figure 6a, layers of organic material and clay (i.e. soft soils) alternate from the ground level to a depth that varies between 5 and 16 m. Subsidence is a widespread problem in the Rotterdam area,

leading to high societal costs, such as adaptation measures in water management and repair costs for damaged buildings and infrastructure. There is ample evidence for this damage, including flooding of cellars, parks and roads, as well as settlement of buildings.

For the area of Rotterdam, the available SAR dataset consists of 285 images acquired via the stripmap mode by the TerraSAR-X constellation of satellites spanning the period 2009-2014. The images are from two separate datasets: 133 from the ascending orbit and 162 from the descending orbit (Peduto et al. 2017c). In particular, analyses focused on two different areas in Rotterdam (Figs. 6b, 6c) wherein 183 buildings are located (125 belong to the first study area and 58 to the second one). As shown in the PSI velocity map of Figure 6b, in these areas the PS located on the top of buildings measured deformation rates higher than 5 mm/year.

As a result of an extensive visual damage inspection carried out in June-July 2016 (Figs. 6c-f), 183 masonry buildings for which PSI data are available, all resting on (mainly wooden) piled foundations, were assigned a damage severity level (Fig. 6c) whose distribution is shown in Figure 6d. Out of 183 buildings, 81 buildings exhibit some level of damage; the number of buildings per damage severity level is: D0 = 102; D1 = 43; D2 = 18; D3 = 11; D4 = 9; D5 = 0.

5.3 Schiedam

The study area is a 2-km^2 densely urbanized neighborhood of the southwestern part of the city of Schiedam, just north of Rotterdam (Fig. 7). The subsoil is composed by a stratified deposit of Holocene age, including layers of clay and peat whose cumulative thickness does not exceed 20 m, laying on a sandy layer (Fig. 7a). Below this sandy layer, soft cohesive soils mix with narrow lenses of sandy soils resting on a sand deposit of Pleistocene age. A sample cross-section of the subsoil in the area, as derived from the GeoTOP model, is shown in Figure 7a.

For the area of Schiedam, the same TSX images over the Rotterdam area were used. The map of PSI data with the measured deformation velocities is shown in Figure 7b.

As for the damage to buildings, in-situ surveys were carried out in April and May of 2015. These surveys focused on 310 single buildings (most of them being part of row-houses) (Fig. 7c) built in masonry – typical of the local architecture – resting on either shallow or piled foundations. Figure 7c shows the map of surveyed buildings distinguished according to their foundation typology (104 shallow and 206 piled) together with the distribution of assigned damage severity levels (Figs. 7d and 7e) and some photos of cracks in building façades and sidewalks taken during the in-situ surveys (Figs. 7f and 7g). The survey of buildings with shallow foundations revealed the existence of 51 buildings with damage; the number of buildings per damage severity level is: D0 = 53; D1 = 21; D2 = 24; D3 = 6; D4 = 0; D5 = 0. Out of the 206 surveyed buildings with piled foundations, 94 buildings with damage were identified; the number of buildings per damage severity level is: D0 = 112; D1 = 56; D2 = 33; D3 = 5; D4 = 0; D5 = 0.

5.4 Dordrecht

Dordrecht is also found in the Rhine Meuse Delta, about 20 km southeast of Rotterdam (Fig. 8a). The subsoil consists mainly of alternating soft cohesive and sandy layers with a few meter thickness each (Fig. 8a). In particular, layers of organic material and clay alternate from the ground surface to a depth that varies between 5 and 12 meters (Peduto et al. 2016a). Typical for this city is the mix of buildings with shallow foundations and (wooden) piled foundations. Substantial land subsidence has taken place in the past, in part related to groundwater lowering. Owing to the damages suffered by the affected buildings, the municipality of Dordrecht fostered an investigation aimed at inspecting the type of foundations and their state of preservation. The same TSX dataset used for Zaanstad allowed the retrieval of PSI data shown in Figure 8b. The sample of surveyed buildings, distinguished according to the assigned damage severity level (Figs.8c-g), consists of 132 masonry structures, of which 76 have a shallow foundation (number of buildings per damage severity level: D0 = 56; D1 = 9; D2 = 5; D3 = 6; D4 = 0; D5 = 0, see Fig.8d) and 56 a piled foundation (number of buildings per damage severity level: D0 = 23; D1 = 16; D2 = 9; D3 = 4; D4 = 2; D5 = 2, Fig.8e).

6. RESULTS

6.1. Phase I and II

Once for each surveyed building the values pertaining to the selected SRI parameters were estimated, they were related to the assigned damage severity level (Phase I-A and I-B in Fig. 2). According to Phase II of the methodology described in section 4, due to similar subsoil settings and properties as well as foundations and structural typology, the results of the four areas were combined into one dataset. This allowed retrieving the empirical relationship between the different SRI parameters and the damage severity levels for a total of 706 masonry buildings (Table 1) with either shallow (180 buildings; Figs. 9.a,c,e,g) or piled (526 buildings; Figs. 9.b,d,f,h) foundations. The values of arithmetic mean (μ) and standard deviation (σ) together with the coefficient of variation CV (defined as σ/μ) per each SRI parameter and damage level are provided in Table 2 for both shallow and piled foundations. The data associated with D4 and D5 damage severity levels were merged in a unique damage class (D4-D5) because the number of buildings falling in these classes was too small for a reliable probabilistic analysis. In this regard, it is worth observing that the highest damage severity level (D4-D5) was recorded only for buildings resting on piled foundations.

On the whole, the obtained relationships show that the damage severity level generally increases as (any of) the selected SRI parameters increase.

6.2. Phase III

In Phase III, by using the cumulative log-normal distribution function (Eq. 1), empirical fragility curves relevant to four SRI parameters were derived for the two foundation types (shallow in Figs.10b, d, f, h and piled foundations in Figs.11 b, d, f, h). For this purpose, the frequency of occurrence of each level of damage severity was calculated for different SRI parameters derived from DInSAR data (see Figs.10a, c, e, g for shallow foundations and Figs.11a, c, e, g for piled foundations). The fragility parameters (i.e. $\overline{SRI_i}$ and β) were computed following the procedure

proposed by Shinozuka et al. (2003) using Equations (2) and (3). The parameters of the corresponding functions are given in Table 3.

7. DISCUSSION

The analyses presented in the above section allowed retrieving empirical relationships and probabilistic functions between a given SRI parameter (among three, one of these computed in two different ways) and the damage severity level based on (monitoring/survey) data collected for 706 masonry buildings on either shallow or piled foundations. The evaluation of the different SRI parameters represents a step forward with respect to previous studies that have introduced the combined use of DInSAR and in-situ damage survey data to generate empirical fragility curves for (differential) settlement-affected buildings (Peduto et al. 2016a, 2017c, 2018b). Indeed, the empirical relationships and probabilistic functions obtained for such a rich dataset suggest hereafter some considerations on the commonly used SRI parameters and the effects on the superstructure associated with their magnitude.

In order to identify the DInSAR-derived SRI parameter – among $\delta\rho$, θ and Δ_1/L_1 (or, equally, Δ_2/L_2) – which, most properly, allows *i)* analyzing the current damage severity level exhibited (on average) by the masonry buildings and *ii)* predicting the damage severity level that might be experienced by a given (i.e. randomly selected) masonry building in the study areas, the values of μ and CV (from empirical relationships) and β (from the fragility curves) for every SRI parameter are compared hereafter.

Focusing on deflection ratios (Δ_1/L_1 and Δ_2/L_2), it can be observed that the empirical relationships (see Figures 9e-h and Table 2) and the fragility curves (see Figures 10e-h and 11e-h) are not markedly influenced by the use of Δ_1/L_1 or Δ_2/L_2. In particular, both series of arithmetic mean, standard deviation and CV (Table 2) as well as the values of fragility parameters (Table 3) referring to different damage severity levels exhibit slight differences whether either Δ_1/L_1 or Δ_2/L_2 is

assumed as SRI parameter. This would suggest that, based on the information on DInSAR data and the damage severity level available in the present study, it could be enough computing the deflection ratio according to the simplified approach (Δ_1/L_1) that does not require the knowledge of all the points of inflection in the cumulative settlement trough along a section of a given building.

Figures 9a-h highlight that $\delta\rho$ seems to be the SRI parameter that works best since its arithmetic mean values can be more easily associated with distinct damage severity levels if compared to the other SRI parameters. Moreover, for each damage severity level and both foundation typologies, the lowest values of CV (associated with the highest precision) are attained for the $\delta\rho$ parameter; whereas the highest ones (associated with the lowest precision) are recorded for the θ parameter. Overall, for a given SRI parameter, almost similar increasing trends of damage severity can be appreciated (on average) for both foundation systems (shallow and piled).

It can also be observed that, for any given SRI parameter, β values (representing the dispersion of the results according to Fotopoulou and Pitilakis 2013) are higher for shallow foundations than for piled ones. This reveals that the considered sample of buildings on shallow foundations is less statistically homogeneous than the one of buildings on piled foundations. Moreover, it is worth noting that for θ, Δ_1/L_1 and Δ_2/L_2 the fragility curves (Figs. 10d, 10f, 10h and Figs. 11d, 11f, 11h) tend to be convex upward in shape (i.e. the existence of an inflection point cannot be clearly recognized), mainly develop horizontally and the probability of reaching or exceeding a given damage severity level can attain the unit value (certainty) for unrealistic values of the considered SRI parameter with respect to limiting values proposed in the literature (Grant et al. 1974, Polshin and Tokar 1957, Skempton and MacDonald 1956). This adversely affects the use of the obtained fragility curves for θ, Δ_1/L_1 and Δ_2/L_2 for forecasting purposes. On the contrary, the fragility curves generated using the $\delta\rho$ parameter for piled foundations (that exhibit all the analyzed levels of damage severity) show that when $\delta\rho$ reaches a value equal to 100 mm the probability of reaching or exceeding D1 to D4/D5 damage level ranges from 90% to 100%. Somewhat surprisingly, values of

$\delta\rho$ higher than approximately 30 mm have only been found for buildings with piled foundations, leading to a higher probability of reaching or exceeding damage severity level D4/D5 than those on shallow foundations. This may be caused by the loss of functionality of single piles due to wood decay processes in correspondence of which settlements concentrate. Apparently, shallow foundations exhibit settlements that are more uniformly distributed (i.e. less localized effects). The more localized settlements of the piled buildings is confirmed by the higher values of θ, Δ_1/L_1 and Δ_2/L_2, which can better explain the damage due to differential settlement.

Comparing the different municipalities, for buildings on shallow foundations (Figs. 9a,c,e,g) SRI parameters attain their minimum values in Schiedam; whereas their maximum values are reached in Dordrecht probably due to the driving force of the groundwater lowering (see section 5.4) which increases the effective stresses pertaining to the subsoil. Buildings in Dordrecht seem to suffer less damage than those in Schiedam for the same value of SRI parameters. Since the considered (subsample of) buildings has homogeneous superstructure and foundation (i.e. shallow) typology the above different behaviour could relate to the specific role played by other factors such as slight differences in the underlying soil deposits and the age of buildings in the two municipalities.

The curves in terms of $\delta\rho$ obtained for the case study at hand were then compared with the ones proposed by Zhang and Ng (2005), who derived empirical fragility curves for a sample of 95 buildings (71 buildings with shallow foundations and 25 on piled foundations). Zhang and Ng (2005) assumed as SRI parameter the maximum vertical settlement (ρ) recorded by a sample of buildings collected in case histories available in the literature and including different structural typologies and varying subsoil conditions. The comparison (Figure 12a and 12b), as expected, highlights that for buildings on both shallow and piled foundations the empirical curves expressed as function of $\delta\rho$ provide probabilities of reaching or exceeding any given level of damage severity that are higher than either limiting tolerable or intolerable settlement (ρ), the latter affecting the functionality/safety of buildings according to Zhang and Ng (2005). This seems to confirm the

different role played by settlements and differential settlements on building damageability. Moreover, it should be noted that the sample of buildings considered by Zhang and Ng (2005) is more heterogeneous since it includes masonry and (more recent) steel and reinforced concrete superstructures that, for a given value of (differential) settlement, can exhibit lower levels of damage severity. On the other hand, DInSAR-derived settlement data, although accurate if compared with traditional settlement markers (see Fig. 1), only cover a period of about 5 years, whereas the damage to the houses may have cumulated over much longer periods, as most of these houses are between 35 and 100 years old. This may have led to an overestimation of the damage category related to the measured parameter. From this point of view, more reliable results might be obtained taking account of some relevant information – such as age of construction, damage severity progress over the time for both interior and exterior bearing walls (provided that knowledge on date of the onset of damage is known) and possible maintenance/repairing/replacing measures during the building life-cycle – not always available for the sample of 706 buildings. Indeed, the assigned damage severity refers to the damage visible only from outside on building façades and only one level was assumed for a single building. Accordingly, further deepening of the presented study is necessary in order to get to a refined analysis**,** including the assignment of a more accurate damage severity level distinguishing hogging or sagging modes of deformations. Moreover, other SRI parameters – such as horizontal strain (Boscardin and Cording 1989) – should be considered, without neglecting the role of tilt (i.e. rigid body rotation) that a building might experience, in concurring to the attainment of serviceability/ultimate limit states. As for horizontal strain, wherever possible, the combination of DInSAR data on both ascending and descending orbits (Peduto et al. 2015, 2017c) would allow the retrieval of the horizontal displacements that could also affect the development of damage in buildings (Boscardin and Cording 1989; Burland et al. 2004).

8. CONCLUSIONS

This paper presented a multi-parameter probabilistic approach for the analysis of damage in masonry buildings with different foundation types (either shallow or piled) in areas where the subsoil mainly consists of soft soils. For the purpose of the analyses, a damage survey dataset resulting from an extensive in-situ campaign of visual inspections was collected over more than 700 masonry buildings located in four municipalities in The Netherlands that for several decades have been dealing with settlement-induced damage to buildings. The damage survey results were combined with three different DInSAR-derived SRI parameters: differential settlement, rotation and deflection ratio (this latter computed in two different ways) over the same sample of buildings in order to derive empirical relationships for the severity level of recorded damage. This allowed enhancing previous studies (Peduto et al. 2016a, 2017c), which were based on the analysis of a single SRI parameter (differential settlement), as well as to identify the SRI parameter (among the selected ones) that is the most suitable to be used for building settlement-induced damage analysis and prediction carried out following the proposed procedure. In particular, the results obtained showed that, as expected, independently of the considered SRI parameter and building foundation typology, the severity level of recorded damage increases as any SRI parameter increases. Moreover, the SRI parameter that best relates with the damage severity level assigned to the considered sample of buildings appears to be the differential settlement. Indeed, it allows an easier and more precise estimation of the damage severity level pertaining (on average) to the investigated sample of masonry buildings and a more realistic predictability (based on the use of fragility curves) of the damage severity level that might be exhibited by a randomly selected masonry building in the study areas.

Main current limitations to a practical applicability of the generated fragility curves would request *i*) a better insight in the development in time of both damage levels and SRI parameters (i.e. the current damage level is compared with the values of SRI parameters referring to a fixed period of time, although those damages may have developed in the past); *ii)* a more detailed damage survey (not limited to outer façade) in order to distinguish the behaviour of portions of buildings in sagging

and hogging zones that could lead to improved performance of the theoretically more correct SRI parameter like Δ_2/L_2.

Notwithstanding the limitations mentioned above, the comparison carried out with empirical fragility curves provided by Zhang and Ng (2005) pointed out the different roles played by settlements and differential settlements on the attainment of a given damage severity level as well as the importance of considering both the exact dating of the onset of damage with respect to the period considered for the computation of cumulative settlements and a homogeneous sample of buildings when performing probabilistic analyses.

Furthermore, the obtained results confirm the capability of DInSAR data to monitor and control the built-up environment with promising benefits in the geotechnical engineering practice. Indeed, gathering the same amount of information through classic monitoring systems would have been unaffordable in terms of both time and money as confirmed by the limited number of buildings analyzed by other scientific works that dealt with the same topic using the outcomes of conventional settlement monitoring data (see section 2 for references therein).

The generated fragility curves, once further validated, could represent a useful tool for local authorities in charge of the management of subsidence-affected urban areas; similarly, they could serve as a warning to house owners on potential damage development, thereby helping in planning adequate foundation repairing/replacing measures before damage reaches intolerable severity levels.

Acknowledgements

The work was carried out under a cooperation within two ERASMUS-traineeship Agreements between the University of Salerno and Deltares and between the University of Salerno and SkyGeo Netherlands B.V. The authors want to acknowledge SkyGeo Netherlands B.V for supplying the DInSAR data and the municipalities of Zaanstad, Rotterdam, Schiedam and Dordrecht for providing the traditional monitoring data and other background information. The MSc students Sonia Colasante, Roberto D'Angelo and Francesco Pastore from the University of Salerno are also

gratefully acknowledged for their contribution to the building damage survey. Finally, the Authors wish to thank the anonymous reviewers and the associate editor who provided useful suggestion for improving the paper in its final version.

REFERENCES

AASHTO 1997. Guide Specifications for Design of Pedestrian Bridges, American Association of State Highway and Transportation Officials, Washington, DC.

Bamler, R. Hartl, P. 1998. Synthetic aperture radar interferometry. Inverse Problems, 14(4): 1–54.

Bjerrum, L. 1963. Allowable Settlement of Structures. Proceedings of the 3rd European Conference on Soil Mechanics and Foundation Engineering, Wiesbaden, 2, Brighton, England, 135–137.

Boscardin, M.D., Cording, E.G. 1989. Building response to excavation induced settlement. Journal of Geotechnical Engineering, 115:1-21.

Bucx, T.H.M., van Ruiten, G., Erkens, G., de Lange, G. 2015. An integrated assessment framework for land subsidence in delta cities. In Proc. IAHS, 372, Prevention and mitigation of natural and anthropogenic hazards due to land subsidence. Copernicus Publications on behalf of the International Association of Hydrological Sciences: 485–491 http://dx.doi.org/10.5194/piahs-372-485-2015.

Burland, J.B., Broms, B.B., de Mello, V.F.B. 1977. Behaviour of foundations and structures. SOA Report, Proc of the 9th Int Conf on Soil Mechanics and Foundation Engineering, Tokyo – Vol. 2, pp. 495-546.

Burland, J.B., Mair R.J., Standing, J.R. 2004. Ground performance and building response due to tunnelling, London. Proc of the Conference on Advances in Geotechnical Engineering, London, Thomas Telford Publisher – Vol. 1, pp. 291-342.

Burland, J.B., Wroth, C.P. 1974. Settlement of buildings and associated damage. SOA Review. Proc of the Conf on Settlement of Structures, Cambridge, Pentech Press, London, pp. 611-654.

Cascini, L., Ferlisi, S., Peduto, D., Fornaro, G., Manunta, M. 2007. Analysis of a subsidence phenomenon via DInSAR data and geotechnical criteria. Italian Geotechnical Journal XLI, 4:50–67.

Cascini, L., Peduto, D., Reale, D., Arena, L., Ferlisi, S., Verde, S., Fornaro, G. 2013. Detection and monitoring of facilities exposed to subsidence phenomena via past and current generation SAR sensors. Journal of Geophysics and Engineering, 10(6):064001. http://dx.doi.org/10.1088/ 1742-2132/10/6/064001.

Castaldo, R., Tizzani, P., Lollino, P., Calo, F., Ardizzone, F., Lanari, R., Guzzetti, F., Manunta, M. 2015. Landslide Kinematical Analysis through Inverse Numerical Modelling and Differential SAR

Interferometry. Pure and Applied Geophysics, 172(11):3067-3080, DOI: 10.1007/s00024-014-1008-3

CEN 2004. Eurocode 7: Geotechnical design - Part 1: General rules. Final Draft, EN 1997-1:2004 (E), (F) and (G), November 2004, European Committee for Standardization: Brussels, 168 pp.

Costantini, M., Falco, S., Malvarosa, F., Minati, F. 2008. A New Method for Identification and Analysis of Persistent Scatterers in Series of SAR Images. IEEE International Geoscience & Remote Sensing Symposium, July 6–11, 2008, Boston, Massachusetts, USA pp. 449–452.

Den Haan, E.J., Kruse, G.A.M. 2006. Characterisation and engineering properties of Dutch peats. In: Tan, T.S., Phoon, K.K., Hight, D.W., Leroueil, S. (Eds.), Characterization and Engineering Properties of Natural Soils 3. Taylor & Francis Group, London, pp. 2101–2133.

DINOloket 2016. Data and information on the Dutch subsurface. Open data portal of the geological survey of the Netherlands. https://www.dinoloket.nl/en (accessed 03.04.2017).
Ferretti, A., Prati, C., Rocca, F., 2001. Permanent scatterers in SAR interferometry IEEE Transactions on Geoscience and Remote Sensing, 39(1):8–20.

Ferlisi, S., Nicodemo, G., Peduto, D. 2018. Empirical fragility curves for masonry buildings in slow-moving landslide-affected areas of southern Italy. In: Kallel A., Ksibi M., Ben Dhia H., Khélifi N. (eds.) Recent Advances in Environmental Science from the Euro-Mediterranean and Surrounding Regions. Proceedings of Euro-Mediterranean Conference for Environmental Integration (EMCEI-1) – Sousse (Tunisia), 22-25 November 2017 – pp. 1825-1828. Advances in Science, Technology & Innovation (IEREK Interdisciplinary Series for Sustainable Development). Springer International Publishing AG, Cham.

Fornaro, G., Reale, D., Verde, S. 2013. Bridge thermal dilation monitoring with millimeter sensitivity via multidimensional SAR imaging. IEEE Geoscience and Remote Sensing Letters, 10:677-68.

Fornaro, G., Reale, D., Verde, S., Peduto, D., Arena, L., Ferlisi, S. 2014. Potentialities of the use of spaceborne radar systems in the monitoring of structures and infrastructures. IEEE Workshop on Environmental Energy and Structural Monitoring Systems (EESMS), Naples, 17–18 September 2014:pp. 69–72 http://dx.doi.org/10.1109/EESMS.2014 (6923267).

Franzius, J.N., Potts, D.M., Addenbrooke, T.I., Burland, J.B. 2004. The influence of building weight on tunneling-induced ground and building deformation. Soils and Foundations, 44(1):25-38.

Gehl, P., Douglas, J., Seyedi D. 2015. Influence of the number of dynamic analyses on the accuracy of structural response estimates. Earthquake Spectra, Earthquake Engineering Research Institute, 31 (1), pp.97-113

Grant, R., Christian, J.T., Vanmarcke, E.H. 1974. Differential settlement of buildings. Journal of the Geotechnical Engineering, ASCE 100, 9:973–991.

Hanssen, F.R. 2003. Subsidence monitoring using contiguous and PS-INSAR: Quality assessment based on precision and reliability. Proc. 11th FIG Symposium on Deformation Measurements, Santorini, Greece pp. 1-8.

Hartemink, A.E., Sonneveld, M.P.W. 2013. Soil maps of The Netherlands. Geoderma, 204–205: 1–9.

Herrera, G., Fernandez-Merodo, J., Tomas, R., Cooksley, G., Mulas, J., 2009. Advanced interpretation of subsidence in Murcia (SE Spain) using A-DInSAR data-modelling and validation. Natural Hazards and Earth System Sciences, 9:647–661.

Holzer, T.L. 2009. Living with Unstable Ground. Environmental Awareness Series American Geosciences Institute Publication, pp. 68 (ISBN: 0-922152-82-9978-0-922152-82-7).

Klaassen, R.K.W.M., Creemers, J.G.M. 2012. Wooden foundation piles and its underestimated relevance for cultural heritage. Journal of Cultural Heritage, 13: 123–128.

Mavrouli, O., Fotopoulou, S., Pitilakis, K., Zuccaro, G., Corominas, J., Santo, A., Cacace, F., De Gregorio, D., Di Crescenzo, G., Foerster, E., Ulrich, T. 2014. Vulnerability assessment for reinforced concrete buildings exposed to landslides. Bulletin of Engineering Geology and the Environment, 73:265-289.

Modoni, G., Darini, G., Spacagna, R.L., Saroli, M., Russo, G., Croce, P. 2013. Spatial analysis of land subsidence induced by groundwater withdrawal. Engineering Geology, 167:59-71, doi:10.1016/j.enggeo.2013.10.014.

Negulescu, C., Foerster, E. 2010. Parametric studies and quantitative assessment of the vulnerability of a RC frame building exposed to differential settlements. Natural Hazards and Earth System Sciences, 10(9):1781-1792.

Nicodemo, G., Peduto, D., Ferlisi, S., Maccabiani, J. 2016. Investigating building settlements via very high resolution SAR sensors. Life-Cycle of Engineering Systems: Emphasis on Sustainable Civil Infrastructure – Bakker, Frangopol & van Breugel (Eds), © 2017 Taylor & Francis Group, London, pp. 2256-2263.

Papadaki, E. 2013. Modeling of Peat Compresses under Sand Bodies: Experimental and Numerical Approach. Master thesis at Technical University Delft, pp. 216. The Netherlands.

Peduto, D., Cascini, L., Arena, L., Ferlisi, S., Fornaro, G., Reale, D. 2015. A general framework and related procedures for multiscale analyses of DInSAR data in subsiding urban areas. ISPRS Journal of Photogrammetry and Remote Sensing, 105:186-210, doi:10.1016/j.isprsjprs.2015.04.001.

Peduto, D., Elia, F., Montuori, R. 2018a. Probabilistic analysis of settlement-induced damage to bridges in the city of Amsterdam (The Netherlands). Transportation Geotechnics, 14:169–182, https://doi.org/10.1016/j.trgeo.2018.01.002.

Peduto, D., Ferlisi, S., Nicodemo, G., Reale, D., Pisciotta, G., Gullà, G. 2017a. Empirical fragility and vulnerability curves for buildings exposed to slow-moving landslides at medium and large scales. Landslides, 14(6):1993–2007, doi: 10.1007/s10346-017-0826-7.

Peduto, D., Huber, M., Speranza, G., van Ruijven, J., Cascini, L. 2017b. DInSAR data assimilation for settlement prediction: case study of a railway embankment in The Netherlands. Canadian Geotechnical Journal, 54(4): 502-517, 10.1139/cgj-2016-0425.

Peduto D., Nicodemo, G., Caraffa, M., Gullà G. 2018b. Quantitative analysis of consequences to masonry buildings interacting with slow-moving landslide mechanisms: a case study. Landslides, 15(10): 2017-2030, DOI 10.1007/s10346-018-1014-0

Peduto, D., Nicodemo, G., Maccabiani, J., Ferlisi, S. 2017c. Multi-scale analysis of settlement induced building damage using damage surveys and DInSAR data: A case study in The Netherlands. Engineering Geology, 218: 117–133, doi: 10.1016/j.enggeo.2016.12.018.

Peduto, D., Nicodemo, G., Maccabiani, J., Ferlisi, S., D'Angelo, R., Marchese, A. 2016a. Investigating the behaviour of buildings with different foundation types on soft soils: two case studies in The Netherlands. VI Italian Conference of Researchers in Geotechnical Engineering, CNRIG2016 -Geotechnical Engineering in Multidisciplinary Research: from Microscale to Regional Scale, 22-23 September 2016, Bologna (Italy). Procedia Engineering, 158:529–534, http://dx.doi.org/10.1016/j.proeng.2016.08.484.

Peduto, D., Pisciotta, G., Nicodemo, G., Arena, L., Ferlisi, S., Gullà, G., Borrelli, L., Fornaro, G., Reale, D. 2016b. A procedure for the analysis of building vulnerability to slow-moving landslides, in: Daponte P, Simonelli AL (Eds.), Proc of the 1st IMEKO TC4 Int Workshop on Metrology for Geotechnics – Benevento, Italy, March 17-18, 2016 – pp. 248-254.

Polshin, D.E., Tokar, R. A. 1957. Maximum Allowable Non-uniform Settlement of Structures. Proc. 4th Int. Conference Soil Mechanics and Foundation Engineering, London, Butterworths Scientific Publications, 402–405.

Reale, D., Fornaro, G., Pauciullo, A., Zhu, X., Bamler, R. 2011. Tomographic imaging and monitoring of buildings with very high resolution SAR data. IEEE Geoscience and Remote Sensing Letters, 8:661–665.

Saeidi, A., Deck, O., Verdel, T. 2012. Development of building vulnerability functions in subsidence regions from analytical methods. Géotechnique, 62(2):107-120, doi: 10.1680/geot.9.P.028.

Shinozuka, M., Feng, M.Q., Kim, H.K., Uzawa, T., Ueda, T. 2003. Statistical analysis of fragility curves. Technical report MCEER-03-0002. State University of New York, Buffalo.

Shinozuka, M., Feng, M.Q., Lee, J., Naganuma, T. 2000. Statistical analysis of fragility curves. J. Eng. Mech., 2000, 126(12): 1224-1231.

Skempton, A.W., MacDonald, D.H. 1956. Allowable settlement of buildings. Proc. of the ICE (Institute of Civil Engineers), Pt. III, Vol. 5, pp. 727–768.

Son, M., Cording, E.J. (2007). Evaluation of building stiffness for building response analysis to excavation-induced ground movements. Journal of Geotechnical and Geoenvironmental Engineering, 133(8):995-1002.

Stafleu, J., Maljers, D., Gunnink, J.L., Menkovic, A., Busschers, F.S. 2011. 3D modeling of the shallow subsurface of Zeeland, the Netherlands. Netherlands Journal of Geosciences-Geologie En Mijnbouw, 90(4):293–310.

USGS, 2016. http://dds.cr.usgs.gov/srtm/ (accessed 03.04.2017).

van der Meulen, M.J., Doornenbal, J.C., Gunnink, J.L., Stafleu, J., Schokker, J., Varnes, R.W.,van Geer, F.C., van Gessel, S.F., van Heteren, S., van Leeuwen, R.J.W., Bakker, M.A.J., Bogaard, P.J.F., Busschers, F.S., Griffiooen, J., Gruijters, S.H.L.L., Kiden, P., Schroot,B.M., Simmelink, H.J., van Berkel, W.O., van der Krogt, R.A.A., Westerhoff, W.E., van Daalen, T.M. 2013. 3D geology in a 2D country: perspectives for geological surveying in the Netherlands. Netherlands Journal of Geosciences-Geologie En Mijnbouw, 92(4):217–241.

Zhang, L.M., Ng, A.M.Y. 2005. Probabilistic limiting tolerable displacements for serviceability limit state design of foundations. Geotéchnique, 55(2):151–161.

Zhu, X., Bamler, R.2010. Very high resolution spaceborne SAR tomography in urban environment. IEEE Transactions on Geoscience and Remote Sensing, 48:4296–4308.

Table 1. Number of surveyed buildings for each study area distinguished according to the foundation type.

Surveyed buildings		
Case studies	**Foundation type**	
	Shallow	**Piled**
Zaanstad	0	81
Rotterdam	0	183
Schiedam	104	206
Dordrecht	76	56
Total	**180**	**526**

Table 2. Arithmetic mean (μ), standard deviation (σ) and coefficient of variation (C_v) of the empirical relationships for each considered SRI parameter distinguished according to the foundation type and damage levels.

SRI parameter	Damage level	Foundation type					
		Shallow			Piled		
		μ	σ	CV	μ	σ	CV
δρ [mm]	D1	6.05	3.42	0.56	6.62	2.90	0.44
	D2	7.71	3.42	0.44	9.38	3.88	0.42
	D3	15.30	4.88	0.32	14.12	4.19	0.30
	D4/D5	-	-	-	25.68	11.93	0.46
θ [rad]	D1	2.16×10^{-4}	3.36×10^{-4}	1.55	2.19×10^{-4}	2.15×10^{-4}	0.98
	D2	1.89×10^{-4}	1.93×10^{-4}	1.02	2.92×10^{-4}	3.93×10^{-4}	1.35
	D3	3.34×10^{-4}	2.00×10^{-4}	0.60	5.21×10^{-4}	5.63×10^{-4}	1.08
	D4/D5	-	-	-	5.15×10^{-4}	5.03×10^{-4}	0.98
Δ_1/L_1 [mm/mm]	D1	2.50×10^{-4}	2.42×10^{-4}	0.97	3.08×10^{-4}	2.20×10^{-4}	0.71
	D2	3.05×10^{-4}	1.66×10^{-4}	0.54	4.20×10^{-4}	2.94×10^{-4}	0.70
	D3	4.80×10^{-4}	3.23×10^{-4}	0.67	6.43×10^{-4}	3.36×10^{-4}	0.52
	D4/D5	-	-		9.44×10^{-4}	4.06×10^{-4}	0.43
Δ_2/L_2 [mm/mm]	D1	2.58×10^{-4}	2.12×10^{-4}	0.82	3.22×10^{-4}	2.14×10^{-4}	0.67
	D2	3.27×10^{-4}	1.71×10^{-4}	0.52	5.98×10^{-4}	3.92×10^{-4}	0.65
	D3	5.37×10^{-4}	3.24×10^{-4}	0.60	6.92×10^{-4}	3.59×10^{-4}	0.52
	D4/D5	-	-	-	1.04×10^{-3}	4.06×10^{-4}	0.39

Table 3. Median ($\overline{SRI_i}$) and standard deviation (β) of the lognormal distribution function for each considered SRI parameter distinguished according to the foundation type and damage levels.

SRI parameter	Damage level	Foundation type			
		Shallow		Piled	
		$\overline{SRI_i}$	β	$\overline{SRI_i}$	β
δρ [mm]	D1	9.04	0.99	12.57	0.57
	D2	25.06	0.99	23.26	0.57
	D3	41.53	0.99	36.81	0.57
	D4/D5	-	-	48.60	0.57
θ [rad]	D1	2.16×10^{-4}	6.04	3.10×10^{-4}	4.14
	D2	4.67×10^{-2}	6.04	8.69×10^{-3}	4.14
	D3	6.38×10^{-1}	6.04	9.08×10^{-2}	4.14
	D4/D5	-	-	1.69×10^{-1}	4.14
Δ_1/L_1 [mm/mm]	D1	3.16×10^{-4}	2.56	5.00×10^{-4}	1.76
	D2	3.26×10^{-3}	2.56	2.21×10^{-3}	1.76
	D3	1.01×10^{-2}	2.56	6.45×10^{-3}	1.76
	D4/D5	-	-	1.26×10^{-2}	1.76
Δ_2/L_2 [mm/mm]	D1	3.46×10^{-4}	2.25	5.32×10^{-4}	1.50
	D2	2.74×10^{-3}	2.25	1.95×10^{-3}	1.50
	D3	7.45×10^{-3}	2.25	5.01×10^{-3}	1.50
	D4/D5	-	-	9.00×10^{-3}	1.50

Figures

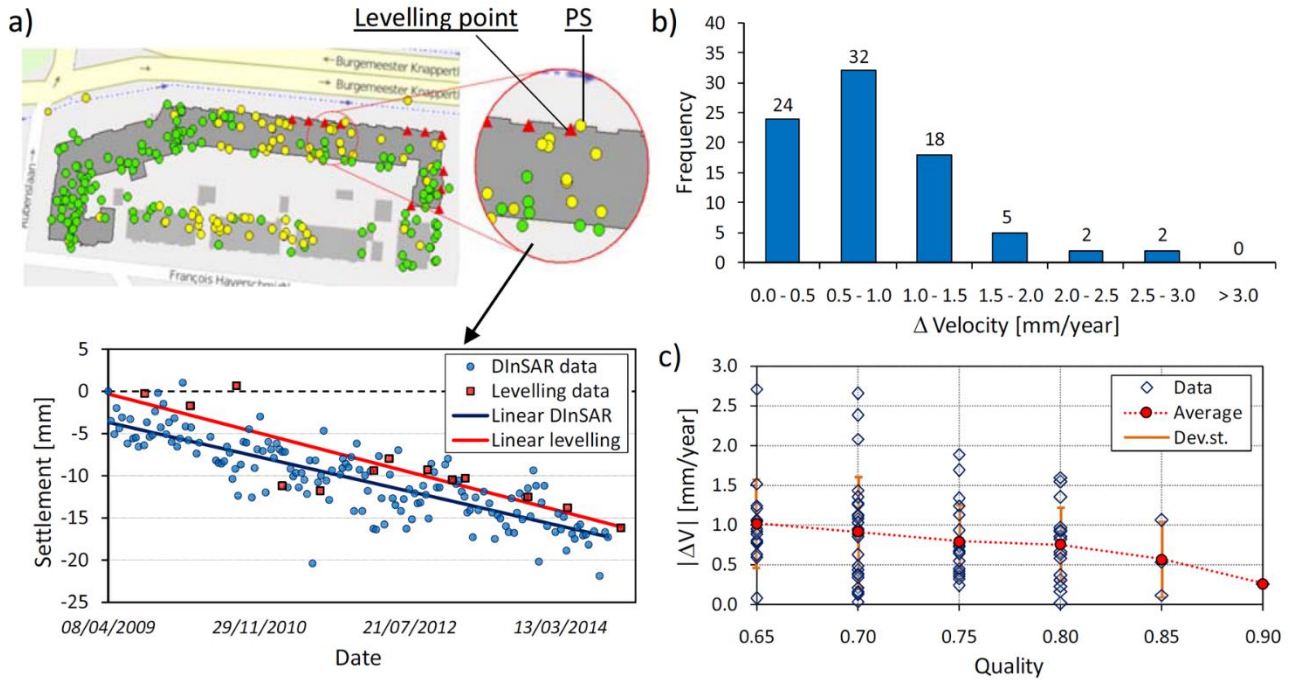

Fig. 1. DInSAR data accuracy test: a) comparison between the time series derived for a levelling benchmark and a PS within 2 m buffer around the levelling point in the period 2009-2014; b) ΔV frequency distribution of the difference between DInSAR and leveling velocities; c) PS quality vs. ΔV recorded in the observation period.

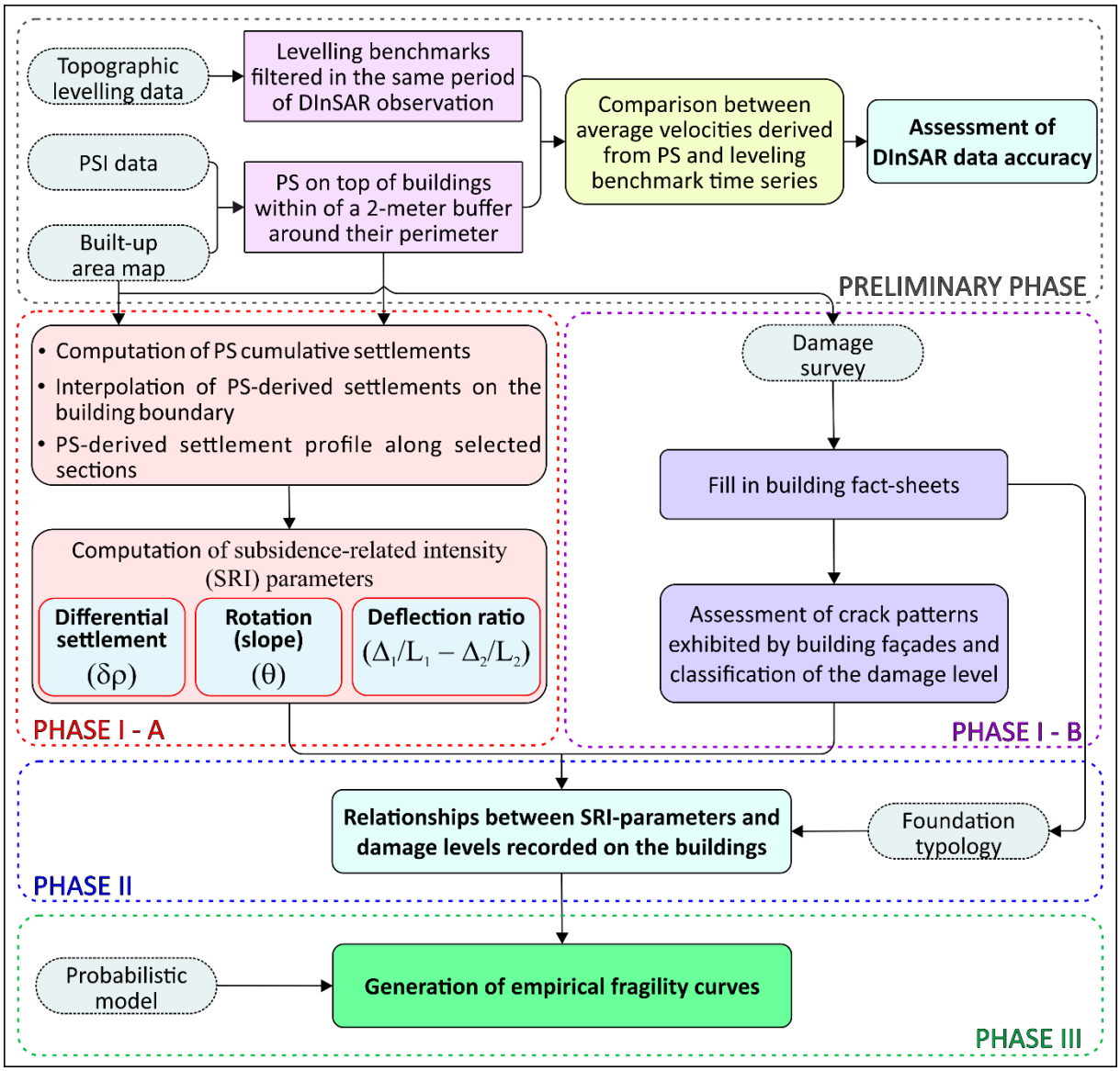

Fig. 2. Flowchart of the methodology.

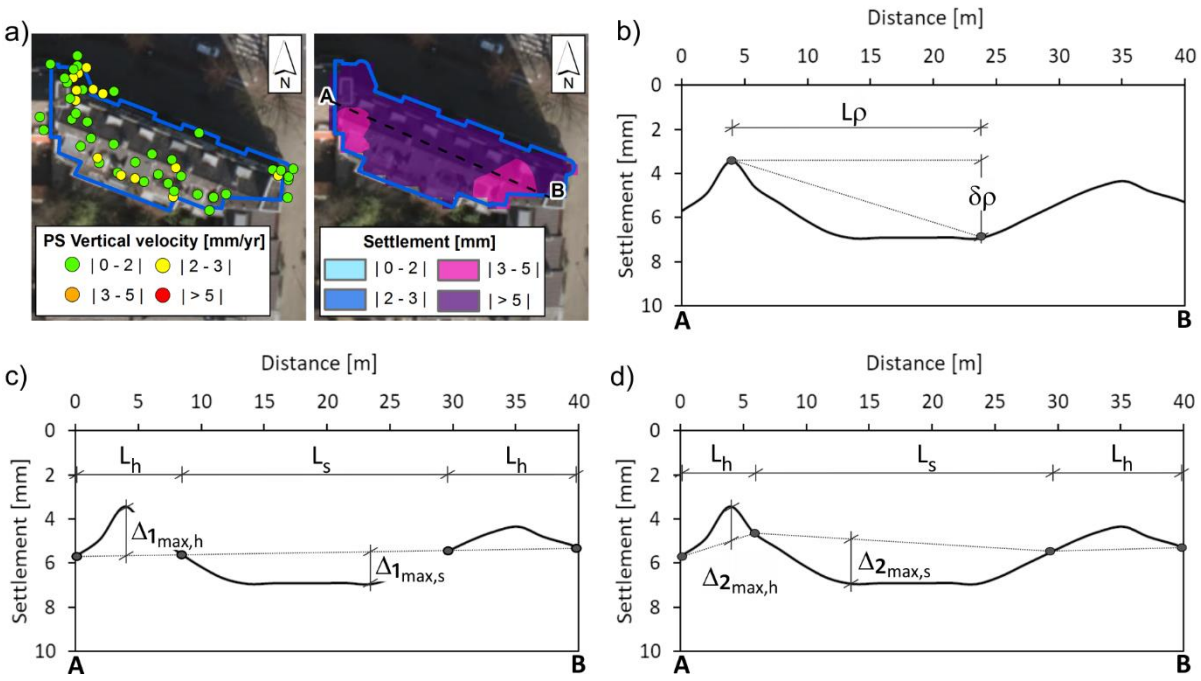

Fig. 3. Sketch synthesizing the computation of the DInSAR-derived SRI parameters: a) map of PS vertical velocity and cumulative settlement; b) differential settlement $\delta\rho$ and $L\rho$; c) deflection ratio as Δ_1/L_1; d) deflection ratio as Δ_2/L_2.

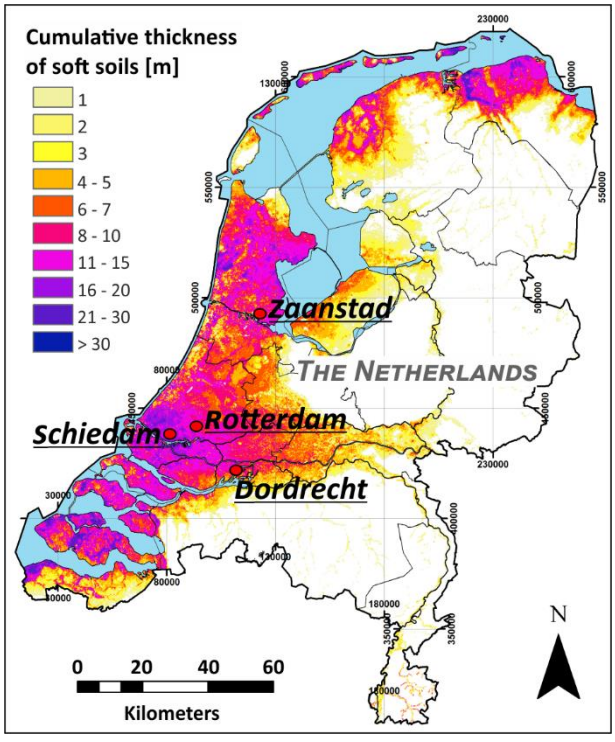

Fig. 4. Location of the case study areas plotted on the map of the cumulative thickness of soft soils in The Netherlands (courtesy of Deltares).

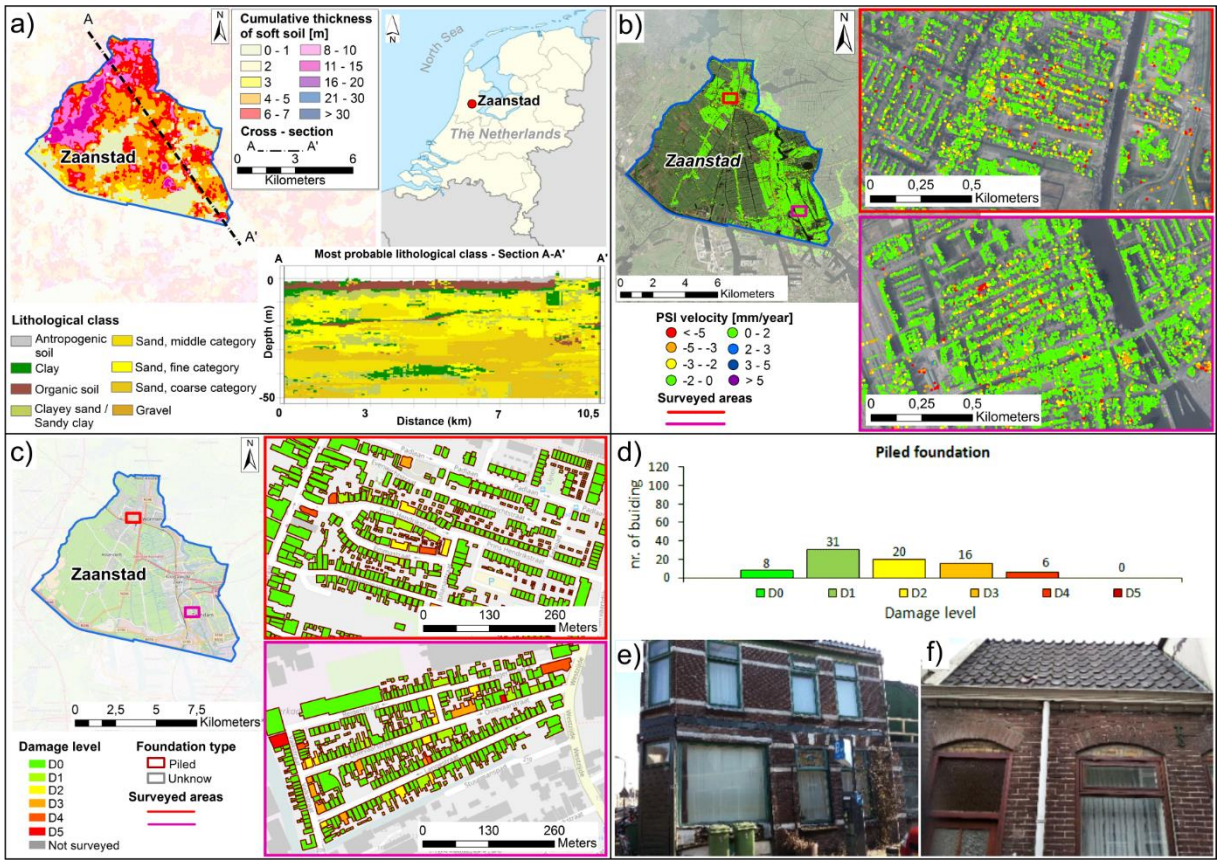

Fig. 5. Zaanstad case study: a) cumulative thickness of soft soils (organic and clayey) and geological cross-section along the A–A' profile sketch; b) PSI data on ascending orbit on top of the buildings provided by the TSX radar sensor; c) map of surveyed masonry building distinguished according to the assigned damage severity level and foundation type and their distribution for d) piled foundations; e) and f) some photos of cracks and deformation revealed on building façades during in-situ surveys.

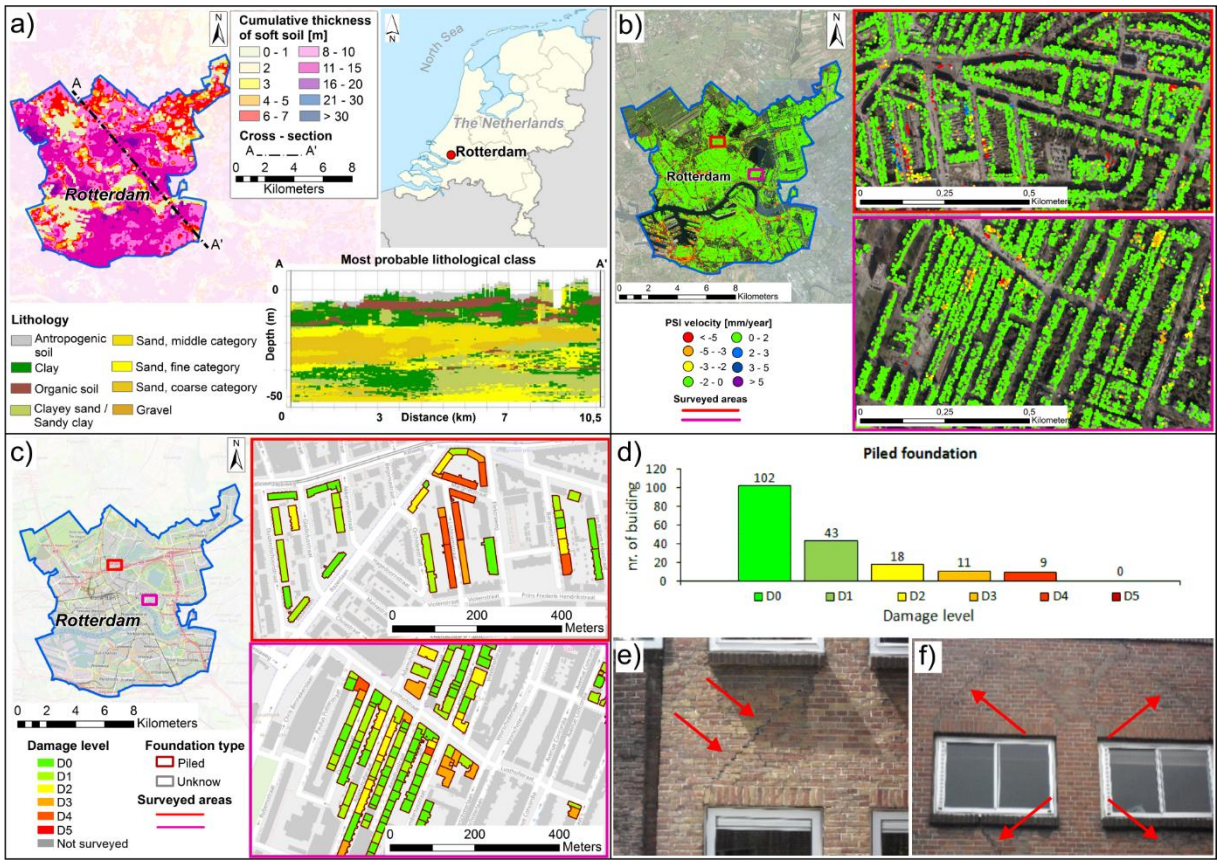

Fig. 6. Rotterdam case study: a) cumulative thickness of soft soils (organic and clayey) and geological cross-section along the A–A' profile sketch; b) PSI data on ascending and descending orbit on top of the buildings provided by the TSX radar sensor; c) map of surveyed masonry building distinguished according to the assigned damage severity level and foundation type and their distribution for d) piled foundations; e) and f) some photos of cracks and deformation revealed on building façades during in-situ surveys.

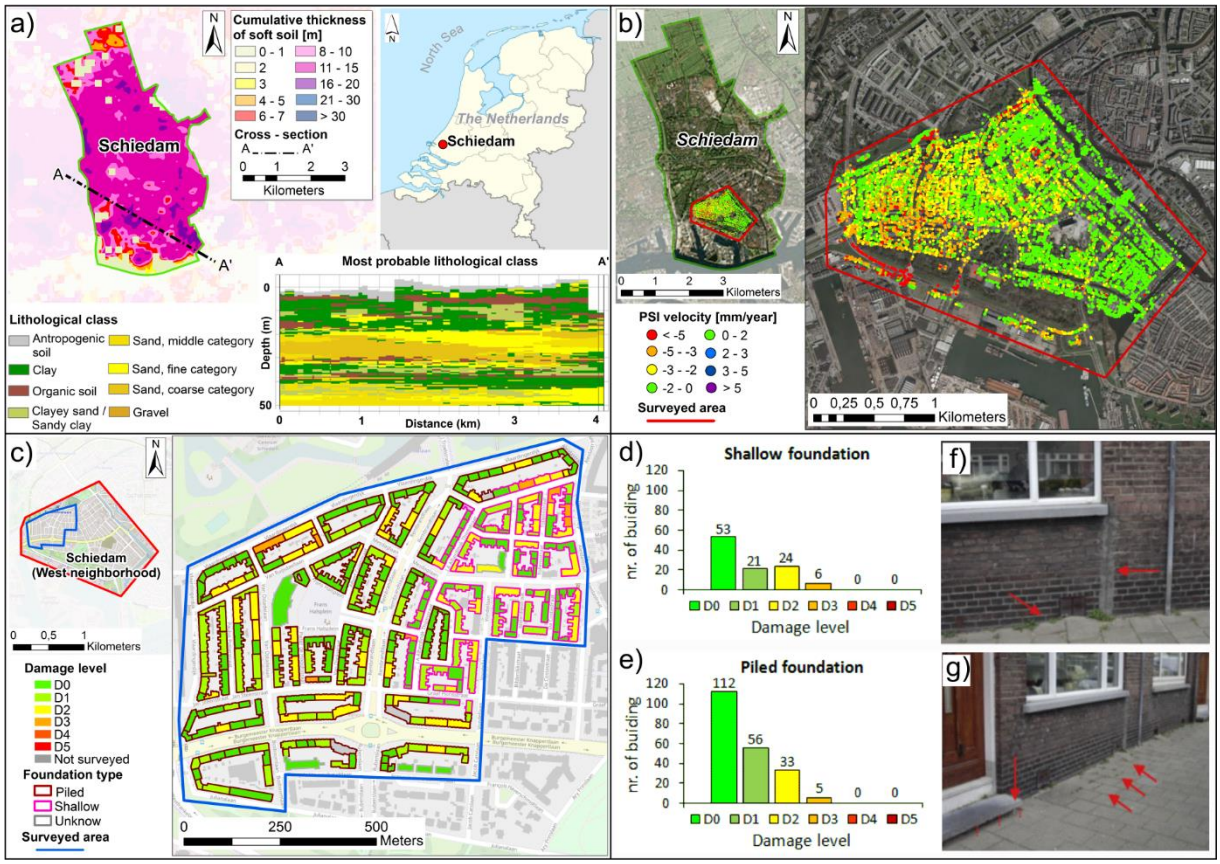

Fig. 7. Schiedam case study: a) cumulative thickness of soft soils (organic and clayey) and geological cross-section along the A–A' profile sketch; b) PSI data on ascending and descending orbit on top of the buildings provided by the TerraSAR-X radar sensor period 2009-2014; c) map of surveyed masonry building distinguished according to the assigned damage severity level and foundation type and their distribution for d) shallow and e) wooden pile foundations; some photos of cracks and deformation revealed during the in-situ surveys on f) building façades g) sidewalks.

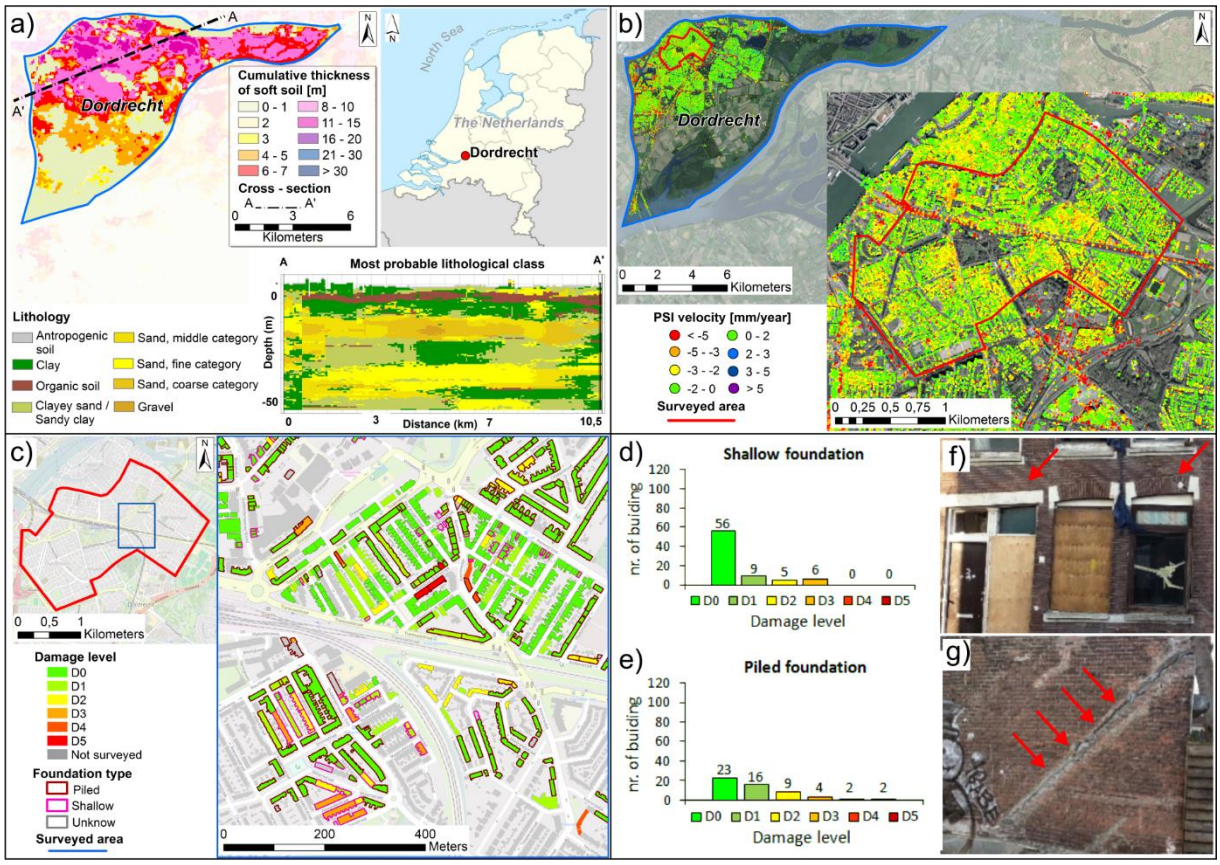

Fig. 8. Dordrecht case study: a) cumulative thickness of soft soils (organic and clayey) and geological cross-section along the A–A' profile sketch; b) PSI data on ascending orbit on top of the buildings provided by the TerraSAR-X radar sensor; c) map of surveyed masonry buildings distinguished according to the assigned damage severity level and foundation type and their distribution for d) shallow and e) piled foundations; f) and g) some photos of cracks and deformation revealed on building façades during in-situ surveys.

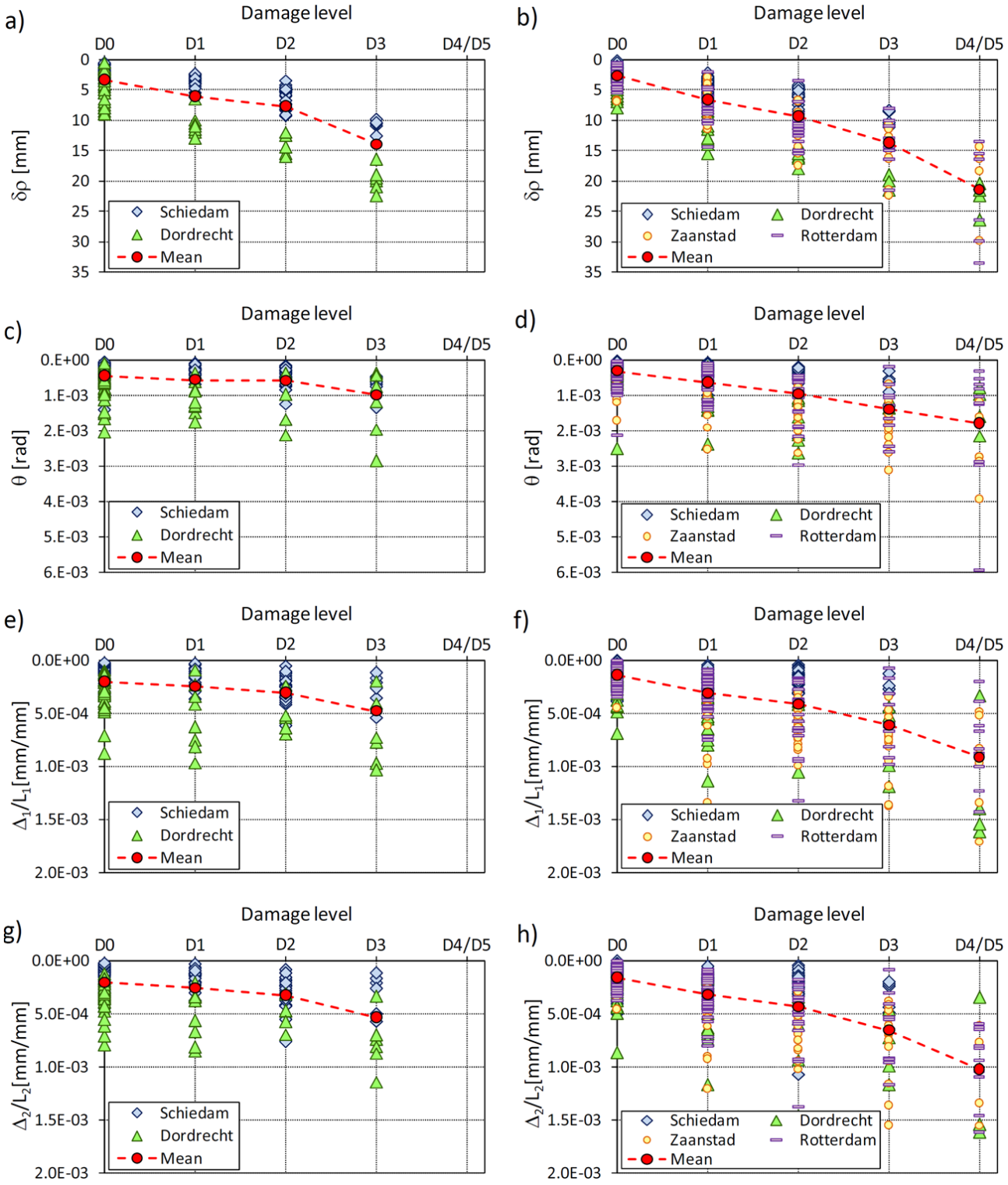

Fig. 9. Damage level vs. SRI parameters for a), c), e), g) shallow and b), d), f), h) piled foundations.

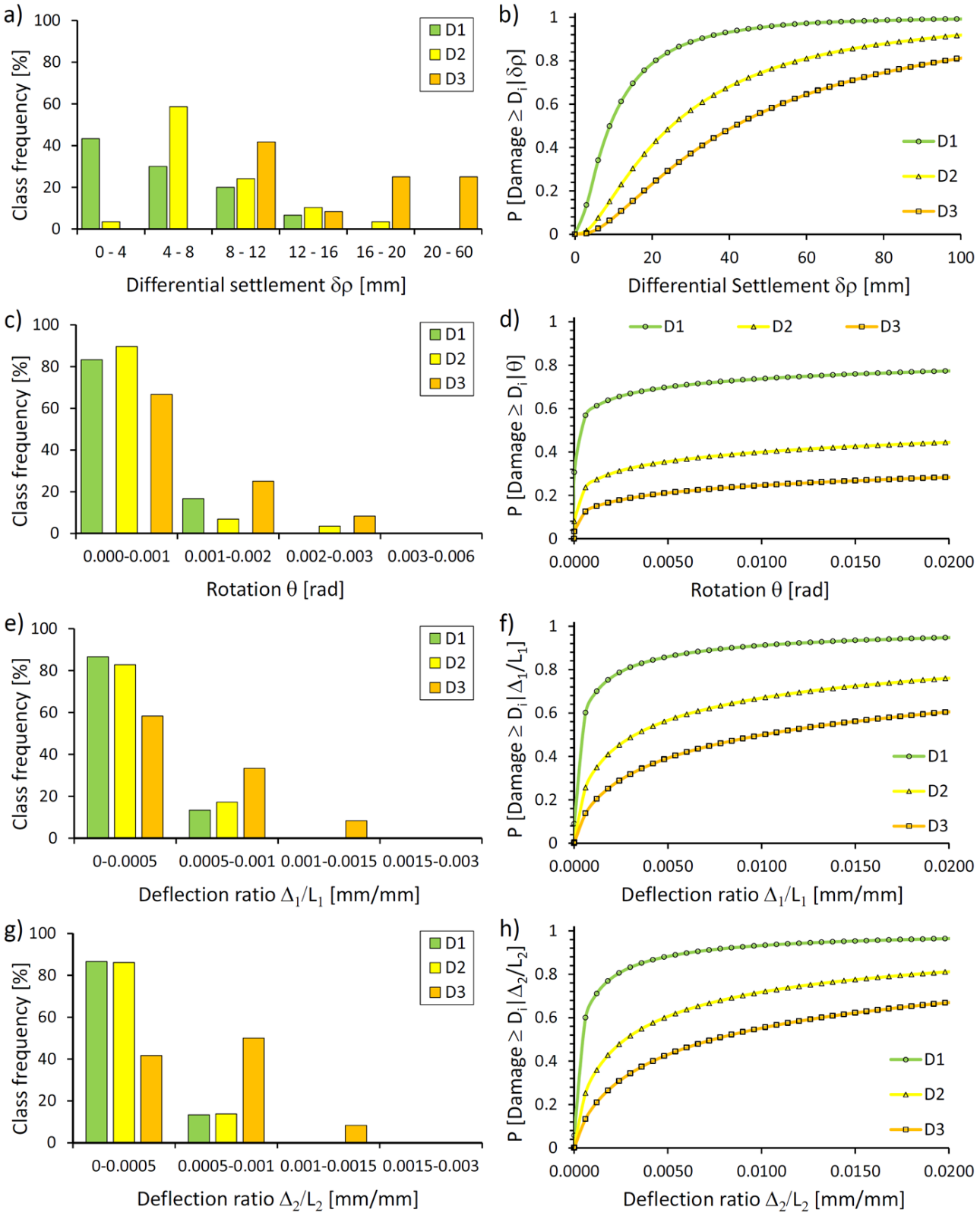

Fig. 10. Results of PSI-derived SRI parameters and damage survey relationship for single buildings with shallow foundation. Class frequency of damage severity level Di assigned to buildings for each considered SRI parameter: a) differential settlement $\delta\rho$, c) rotation θ, e) deflection ratio Δ_1/L_1, g) deflection ratio Δ_2/L_2; fragility curves generated by using the log-normal distribution function for

each considered SRI parameter: b) differential settlement δρ, d) rotation θ, f) deflection ratio Δ_1/L_1, h) deflection ratio Δ_2/L_2.

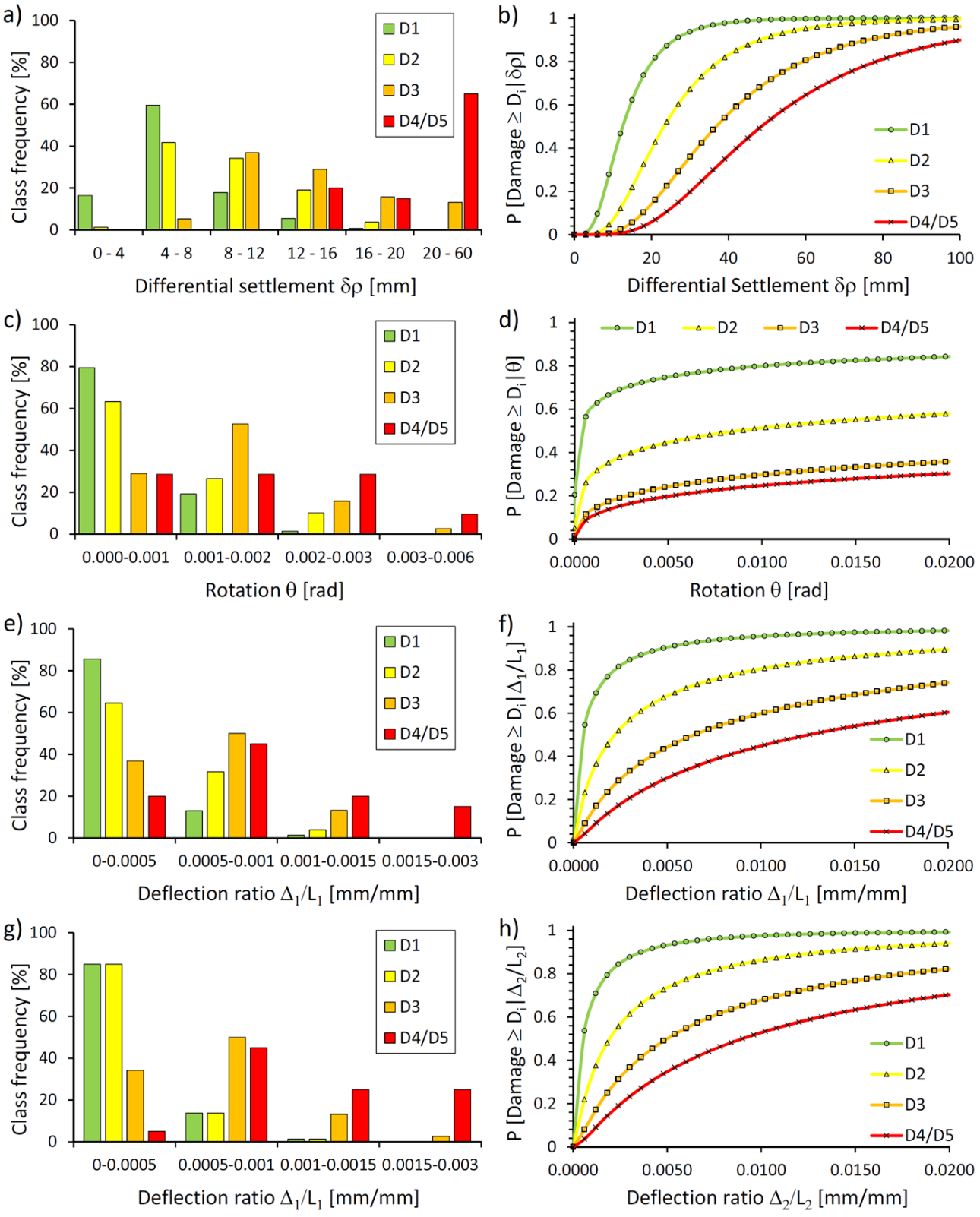

Fig. 11. Results of PSI-derived SRI parameters and damage survey relationship for single buildings with piled foundation. Class frequency of damage severity level Di assigned to buildings for each

considered SRI parameter: a) differential settlement δρ, c) rotation θ, e) deflection ratio Δ_1/L_1, g) deflection ratio Δ_2/L_2; fragility curves generated by using the log-normal distribution function for each considered SRI parameter: b) differential settlement δρ, d) rotation θ, f) deflection ratio Δ_1/L_1, h) deflection ratio Δ_2/L_2.

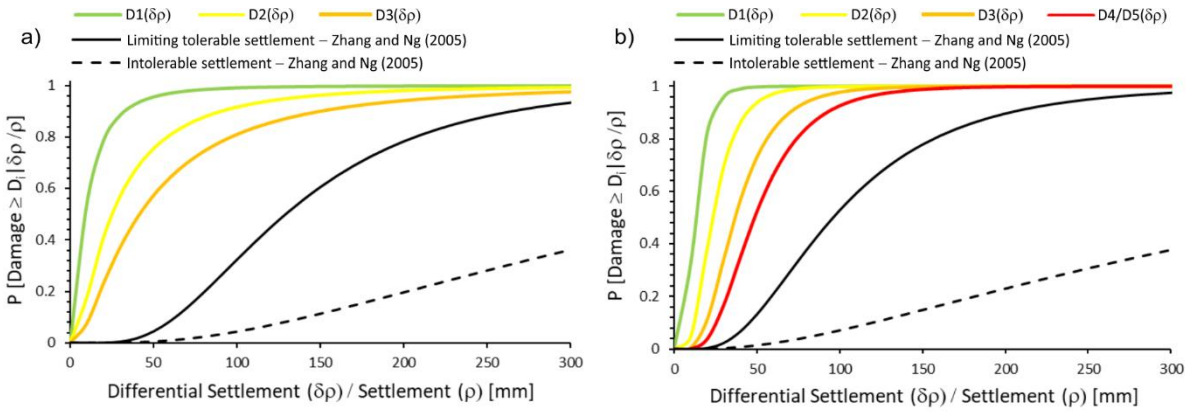

Fig. 12. Comparison of the proposed empirical fragility curve as a function of differential settlement (δρ) with the empirical curves as a function of settlement (ρ) provided by Zhang and Ng (2005) for a) buildings with shallow foundations and b) buildings with piled foundations.